JOURNAL OF MAGNETIC RESONANCE IMAGING 14:540–546 (2001)

Original Research

Improved High Resolution MR Imaging for Surface Coils Using Automated Intensity Non-Uniformity Correction: Feasibility Study in the Orbit

Elizabeth A. Vokurka,[1] Nick A. Watson,[1] Yvon Watson,[1] Neil A. Thacker,[1] and Alan Jackson[1]*

This study examined the effects of a recently developed automated intensity non-uniformity correction on surface coil images using the orbit as an exemplar. Images were obtained using a standard head coil and a range of surface coils. Slices through the optic nerve head and cavernous sinus were subjected to the correction algorithm. Blind forced-choice rankings of the subjective image quality were performed. Quantitative measurements were taken of the similarity between vitreous humor at two depths from the coil, and of the conspicuity between orbital fat and temporalis muscle intensities. The combined qualitative ranks for corrected surface coil images were higher than for the equivalent uncorrected images in all cases. Intensity non-uniformity correction produced statistically significant improvements in orbital surface coil images, bringing their intensity uniformity in homogeneous tissue to the level of head coil images. The subjective quality of the corrected surface coil images was superior to head coil images, due to increased spatial resolution combined with improved signal to noise ratio across the image. J. Magn. Reson. Imaging 2001;14:540–546. © 2001 Wiley-Liss, Inc.

Index terms: intensity non-uniformity correction; orbital imaging; surface coils; image processing; high resolution imaging

IMAGING OF SUPERFICIAL ORBITAL structures is best performed using surface coils to increase signal-to-noise ratio (1–5). However, many MR centers routinely perform orbital imaging using head coils to ensure adequate visualization of posterior orbital structures (6–8).

The use of orbital phased arrays provides a compromise but is limited to a small number of specialist centers due to cost and commercial availability (9). Mapping of surface coil non-uniformity using fluid phantom or mathematical models can be used to correct for large inhomogeneities but does not allow for variations in coil placement (10,11). This is particularly important with flexible surface coils where accurate alignment of phantom and clinical data becomes impossible. The use of a post-processing technique is therefore attractive; however most rely on tissue classification or modeling and require some level of expert supervision (12–14).

We have recently described in this journal a post-processing algorithm designed to automatically detect and correct for non-uniformity in images resulting from receiver coil heterogeneity (15). This non-parametric algorithm assumes that coil heterogeneity will result in smooth shifts in intensity, which can be detected within homogeneous tissue. It provides a robust, computationally fast method of intensity correction that is independent of coil geometry and tissue content. The corrected image displays improved statistical consistency of single tissue signal intensity within homogeneous tissue. Although it was not originally intended for use on surface coil images, we noted a subjective improvement in such images in our preliminary studies.

The aim of this study is to examine the quality and statistical properties of non-uniformity corrected images obtained with surface coils. Because of the specific problems associated with surface coil images of the orbit, this has been chosen as a clinical exemplar.

MATERIALS AND METHODS

Scanning

Imaging was performed on a 1.5 Tesla scanner (ACS-NT PT6000 Philips Medical Systems). Imaging was performed in a single normal male volunteer. In all cases, the orbit was scanned using a three-dimensional T1-weighted, gradient echo sequence (TR 30 msec, TE 8.6 msec, flip angle 30 degrees). The images were acquired with a matrix of 256 × 256, resulting in in-plane pixel resolution of 0.35 × 0.35 mm and a 9-cm field of view to cover the whole orbit and the cavernous sinus. The field-of-view and matrix size remained constant for all sequences. The body coil was used as the RF transmitter for all scans. Images were obtained using the standard head coil, a flexible 8-cm circular surface coil (C4),

[1]Division of Imaging Science and Biomedical Engineering, Department of Medicine, University of Manchester, Manchester, UK.

Contract grant sponsor: European Commission project: NOVICE (Network Oriented Visualisation in a Clinical Environment), ESPRIT; Contract grant number: EP26342.

*Address reprint requests to: A.J., Division of Imaging Science and Biomedical Engineering, Department of Medicine, Stopford Building, University of Manchester, Manchester, M13 9PT, UK.
E-mail: alan.jackson@man.ac.uk

Received February 5, 2001; Accepted July 16, 2001.

and two miniature circular coils with diameters of 5-cm (C5) and 2.5-cm (C6). In order to produce linear variation in the signal to noise characteristics of the images, five acquisitions were performed with each coil, varying the slice thickness from 2- to 6-mm in 1-mm increments (16).

Non-Uniformity Correction Technique

A slice showing the optic nerve and cavernous sinus from each image volume was chosen for comparison. Each selected slice was subjected to an intensity non-uniformity correction (15) that can be found in the open source algorithmic development software package, TINA (17). This intensity shift is estimated across the image in two orthogonal directions, taking into consideration statistical accuracy of signal intensity and its derivatives at each voxel as in Eq. [1].

$$\Delta_x^S(x,y) = \frac{S \otimes (\Delta_x^{rel}\sigma_x^{-2}(x,y) + 0)}{S \otimes (\sigma_x^{-2}(x,y) + \sigma_{reg}^{-2})} \quad (1)$$

$\Delta_x^S(x,y)$ is the smooth local x-derivative at a given point. $\otimes$ represents a two-dimensional convolution with an exponential infinite impulse response filter, S. Δ_x^{rel} is the x-derivative relative to intensity. σ_x is the estimated error in the derivative measurement using estimates of pixel intensity error. σ_{reg} is a regularization term that constrains the effects of large errors in the appropriately weighted mean equation. Re-integration of the two resultant derivative images provides a multiplicative correction map for the overall intensity inhomogeneity in the image.

Qualitative Comparison of Image Quality

The images were assessed for subjective quality by two experienced orbital radiologists. All images were randomly assigned an identifying number. These identifiers were used to blind the observers to the slice thickness, imaging coil, and correction status throughout the analysis. A software tool was developed (18) to sequentially display each of the 40 images in random pairings, resulting in 780 comparisons ($40 \times [40-1] \div 2$). The image quality was assessed as better in one image or differentiation not possible. Each viewer performed the scoring twice to compare the image quality at the optic nerve head and cavernous sinus independently to provide scores representative of superficial and deep structures. To determine intra-observer error in the method, one observer ranked images of the optic nerve head on two separate occasions. Weighted mutual rankings (R_i) of the two anatomical regions were determined for each observer which were the average of the individual ranking systems corrected to allow for the absolute range of each:

$$R_i = \frac{N}{M}\sum_{j=1}^{M}\frac{r_{ij}}{r_{\max j}} \quad (2)$$

where j is the coil and slice thickness to be ranked, N the number of coil and slice thickness combinations (i.e., image pairs compared), M the number of ranks to be combined, r_{ij} the individual rank for a specific coil and slice thickness, and $r_{\max\ j}$ the maximum rank for specific coil and slice thickness.

The weighted mutual rankings were averaged over the two observers and anatomical regions to provide a final rank. Inter- and intra-observer agreement was estimated by use of a Spearman's rank coefficient and differences were assessed by measurement of the weighted Cohen's kappa statistic (18).

Quantitative Measurement of Tissue Contrast

While ranking of image quality provides an indication of clinical value in an image, it cannot be used as a measure of the overall image quality for image processing techniques such as automated segmentation. To compare the image characteristics in identical tissue at varying depths, the mean and variance of signal intensity in the anterior and posterior globe were calculated for each image. These were used to calculate the position at which the distributions of the regions of interest intersect. This measurement was expressed in units of SD from mean intensity of the region of interest deep in the globe and provides an index of the similarity of the two regions of interest. To estimate the contrast (conspicuity), between two different tissues at comparable depth from a surface coil, the distribution of intensity in regions of interest were measured in the fat at the midpoint of the orbit and in temporalis muscle. This data was again used to calculate the position at which the distributions of the regions of interest intersect. This measurement was expressed in units of SD from mean intensity of the temporalis muscle sample. This estimate of conspicuity provides similar information to a pooled variance but has the advantage of being effective even when the distributions are greatly separated.

Figure 1A provides an example of the similarity and conspicuity regions of interest. Both measurements were taken with regions of interest of comparable size. Noise was calculated as the SD of the distribution of x- and i-derivatives using a (–1,0,1) kernel at each voxel within a given region. The mean of the distribution was taken as the mean signal intensity. The signal-to-noise ratio of an image is an important index of image quality. In general terms, this can be described as the ratio of intensity to noise of homogeneous tissue. In surface coil images, the spread of the distribution will vary with the depth from the coil due to signal drop-off. The noise term can be split into two linearly related components.

$$SNR = \frac{I}{\sigma_{noise} + \sigma_{signal\ dropoff}} \quad (3)$$

The intensity correction algorithm should remove the effect of the variance due to signal drop-off, ($\sigma_{signal\ drop\text{-}off}$). While the inherent noise in the image, (σ_{noise}), is boosted due to the correction at depth, the resultant distribution is significantly sharper than an equivalent distribution in the uncorrected image (15).

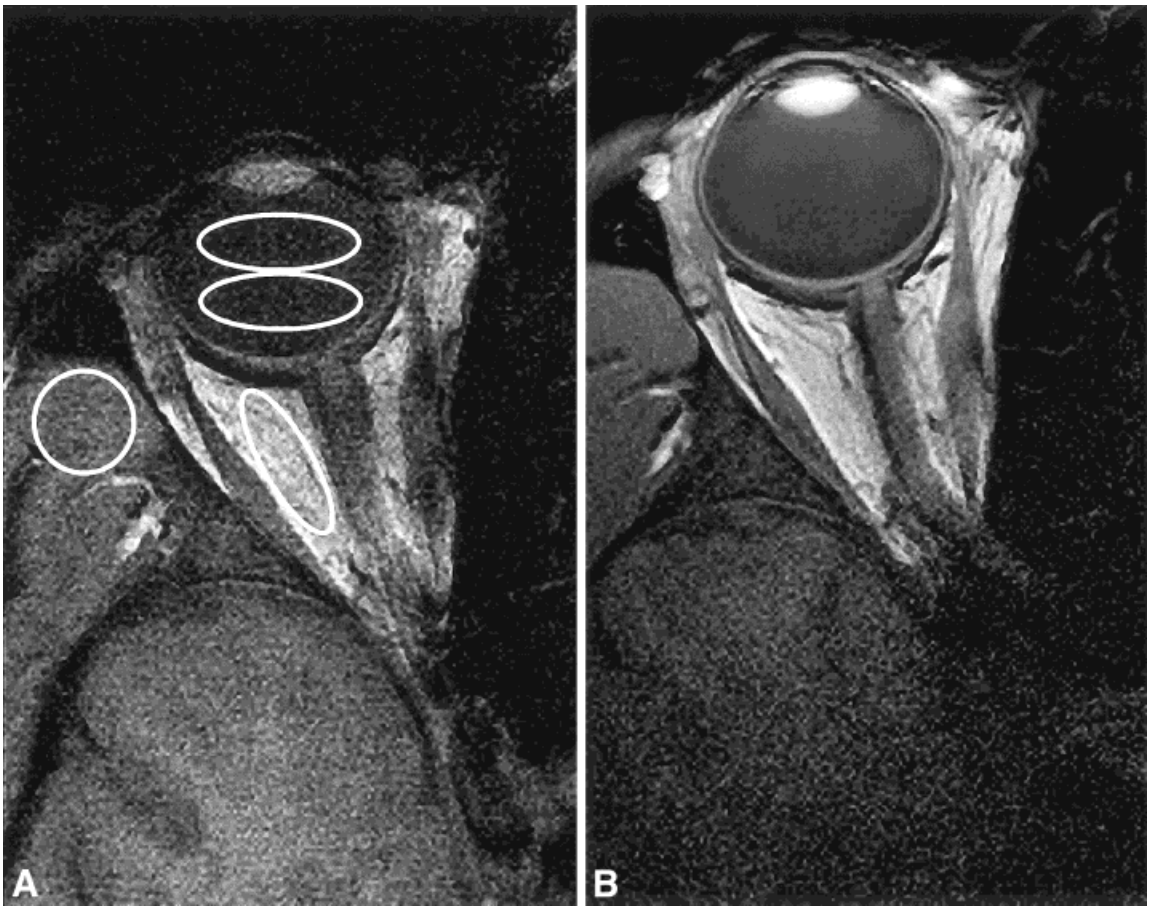

Figure 1. A: The best image of the optic nerve head using the head coil (5-mm slice thickness). This image illustrates the regions of interest used for measuring similarity (vitreous humor at two depths) and conspicuity (retro-orbital fat and temporalis muscle). **B:** The best overall image of the optic nerve head, acquired with a 3-mm slice thickness image using the 2.5-cm diameter surface coil. The image was non-uniformity corrected.

RESULTS

Qualitative Comparison of Image Quality

The results of the rankings are shown in Table 1. The uncorrected 5-mm slice thickness head coil provided the best visualization in the region of the globe for all head coils (Fig. 1A). Inter-observer mutual ranking for the quality of the optic nerve alone indicated that the best image choice was the non-uniformity corrected, 3-mm slice thickness image obtained with the 2.5-cm coil (Fig. 1B). Comparison of the image rankings for the two observers produced a rank correlation coefficient of $R^2 = 0.958$ ($P < 0.001$); weighted Cohen's kappa was 0.89. Repeated rank scoring by one observer demonstrated a rank correlation coefficient of $R^2 = 0.952$ ($P < 0.001$); weighted Cohen's kappa = 0.910.

The small 5-cm and 2.5-cm surface coils were unable to demarcate the cavernous sinus in most cases. For the remaining images, the uncorrected 5-mm slice head coil images provided the clearest image of the cavernous sinus and orbital apex. The highest-ranking surface coil image was the corrected 6-mm thick slice from the 8-cm coil, which ranked 8th out of 40. Comparison of the image rankings for the two observers produced a rank correlation coefficient of $R^2 = 0.912$ ($P < 0.001$); weighted Cohen's kappa was 0.86.

The ranking for non-uniformity corrected surface coil images was higher than for the equivalent uncorrected images in all cases. Mutual rankings for both observers and both anatomical regions were calculated, indicating the optimal single sequence in terms of subjective image quality in the superficial and deep orbit. The head coil produced the highest inter-observer mutual ranking for uncorrected images. The highest overall mutual ranking was produced by the non-uniformity corrected, 4-mm slice thickness image from the 5-cm diameter coil (Fig. 2).

Quantitative Measurement of Tissue Contrast

The similarity between signal intensity from the anterior and posterior regions of the globe in uncorrected and corrected head coil and 8-cm surface coil images were well within the statistical limits of a single distribution (Fig. 3). The uncorrected 5-cm surface coil images showed significant separation in intensity distribution with respect to the depth of the tissue, especially with thick acquisition slices. After non-uniformity correction, the mean intensities of the two regions of the globe were within 2 SD, indicating that non-uniformity correction produced significant improvement in signal drop off so that the

Table 1
Results of the Image Comparisons For the Optic Nerve, Cavernous Sinus and For Both Areas Combined

Optic nerve	Weighted mutual rank optic nerve	Cavernous sinus	Weighted mutual rank cavernous sinus	Mutual score	Weighted mutual rank overall
3mm C6 N	*2.13*	4mm H	*1.95*	***4mm C5 N***	*10.77*
2mm C5	2.68	6mm H	2.90	***6mm C5 N***	12.79
2mm C5 N	2.77	***4mm H N***	2.90	***6mm C4 N***	14.30
2mm C6 N	4.06	5mm H	3.90	***5mm C4 N***	14.87
4mm C6 N	6.19	***6mm H N***	5.86	***2mm C5 N***	16.00
4mm C5 N	6.83	***5mm H N***	6.90	***5mm C5 N***	16.01
3mm C5 N	8.03	***3mm H N***	7.81	***3mm C5 N***	16.18
6mm C5 N	8.96	***6mm C4 N***	7.90	5mm H	16.36
3mm C5	9.41	3mm H	10.76	4mm H	17.42
4mm C5	10.16	***5mm C4 N***	11.81	6mm H	17.52
6mm C5	10.99	***5mm C5 N***	12.71	***4mm H N***	17.62
2mm C6	11.83	***4mm C5 N***	14.71	***4mm C6 N***	17.74
5mm C6 N	13.02	***6mm C5 N***	16.62	***5mm H N***	18.18
3mm C6	15.15	***4mm C4 N***	19.67	***3mm C6 N***	18.63
5mm C5	17.28	2mm H	20.48	***2mm C6 N***	20.05
5mm C4 N	17.92	***2mm H N***	21.52	***6mm H N***	20.16
3mm C4	18.38	***3mm C5 N***	24.33	***5mm C6 N***	20.23
5mm C5 N	19.31	***5mm C6 N***	27.43	2mm C5	20.86
3mm C4 N	19.76	5mm C4	28.52	***4mm C4 N***	21.94
5mm C4	20.50	6mm C4	28.57	***3mm H N***	22.89
6mm C4 N	20.69	***2mm C5 N***	29.24	5mm C4	24.51
6mm C6 N	21.53	***4mm C6 N***	29.29	6mm C5	24.52
6mm C4	21.98	***2mm C4 N***	29.33	3mm C5	24.71
4mm C4	23.37	***3mm C4 N***	30.43	4mm C5	25.08
4mm C4 N	24.21	4mm C6	30.43	***3mm C4 N***	25.09
2mm C4 N	26.05	4mm C4	32.38	6mm C4	25.28
2mm C4	26.98	3mm C4	33.33	3mm H	25.38
5mm H	28.82	***3mm C6 N***	35.14	3mm C4	25.85
5mm H N	29.46	***6mm C6 N***	35.19	2mm C6	25.91
5mm C6	29.65	***2mm C6 N***	36.05	3mm C6	27.57
4mm C6	29.84	6mm C5	38.05	***2mm C4 N***	27.69
6mm C6	31.97	2mm C4	38.10	4mm C4	27.88
6mm H	32.14	5mm C6	39.00	***6mm C6 N***	28.36
4mm H N	32.33	6mm C6	39.00	5mm C5	28.64
4mm H	32.88	2mm C5	39.05	2mm H	29.17
6mm H N	34.46	3mm C5	**40.00**	4mm C6	30.14
2mm H	37.87	4mm C5	**40.00**	***2mm H N***	30.44
3mm H N	37.97	2mm C6	**40.00**	2mm C4	32.54
2mm H N	39.35	3mm C6	**40.00**	5mm C6	34.33
3mm H	**40.00**	5mm C5	**40.00**	6mm C6	**35.49**

The table shows the coil used and whether the image was normalized. The associated mutual ranking score for each observer is also shown. N, normalized image; H, head coil. Coli combinations in bold italics indicate that intensity non-uniformity correction was applied. Rankings in bold indicate the maximal ranking achieved.

measures became statistically similar. Uncorrected images from the 2.5-cm surface coil showed significant separation of the distributions, greater than that observed with other coils. Intensity non-uniformity correction did improve the homogeneity of these images, but only to the similarity level of the uncorrected 5-cm surface coil.

The conspicuity measurement between orbital fat and temporalis muscle was insignificant (a conservative estimate of 2 SD or less from the mean intensity) for uncorrected and non-uniformity corrected head coil images and for all uncorrected surface coil images (Fig. 4). Only non-uniformity corrected images obtained with surface coils consistently provide statistically significant contrast between the mid retro-orbital fat and temporalis muscle.

DISCUSSION

Surface coils provide higher spatial resolution orbital images while maintaining the signal-to-noise ratio at levels comparable to those seen with volume coils (9,18–20). However, decrease in signal-to-noise ratio distant to the coil limits their use in clinical applications where imaging of deeper structures is also required (6,7). The prominent component of the noise in these cases is the rapid intensity drop-off seen in surface coil images. This produces broadening of the intensity distribution of otherwise homogeneous tissues (15,19). This effect is potentially correctable if the non-uniformity characteristics of the image are known. In images obtained with surface coils the major cause of intensity non-uniformity is the sensitivity profile of the coil itself.

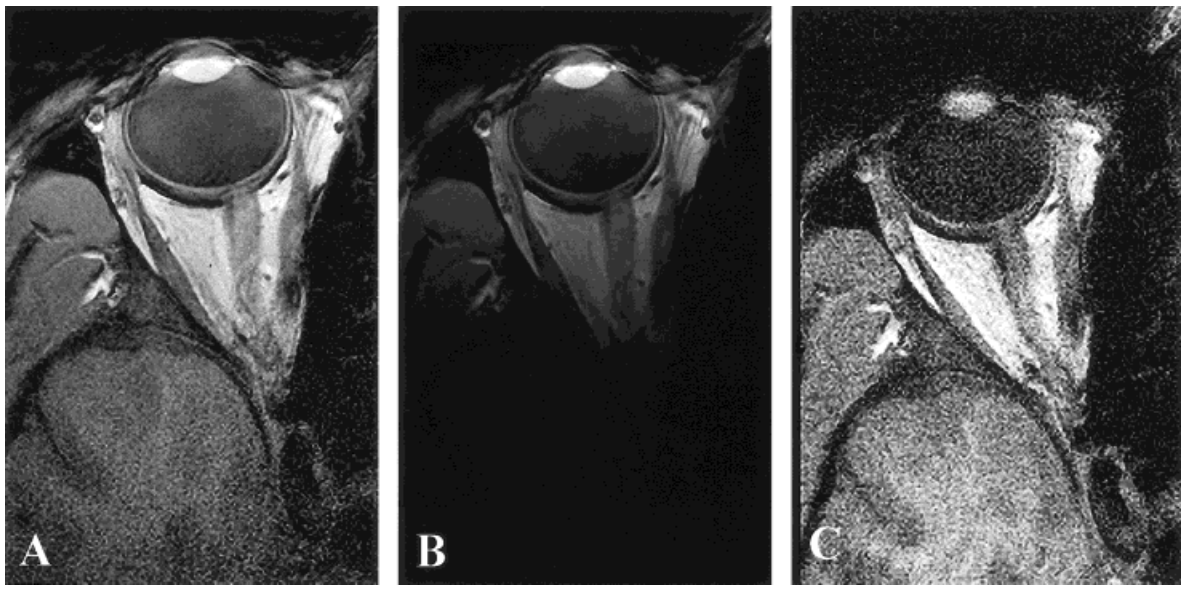

Figure 2. The top mutually ranked image using non-uniformity correction of an image with a slice thickness of 4 mm acquired using a 5-cm surface coil. **B:** The image (**A**) before non-uniformity correction. **C:** The best ranked head coil image using the mutual ranking score.

The apparent subjective improvement in intensity non-uniformity corrected surface coil images was noted in our previous work (15). Clearly the algorithm cannot improve the true signal-to-noise ratio of the image, and the basis of these apparently dramatic improvements in subjective image quality was unclear. The present study has attempted to clarify the mechanism of the improvement and to objectively examine whether the subjective change in image quality represents a true measurable change in image quality. The measurements of similarity in the globe demonstrated the expected loss of tissue homogeneity with surface coil images due to coil related signal drop-off as the distance of the measurement point from the surface coil increased. This effect was least marked with the largest surface coil and greatest with the smaller 5- and 2.5-cm-diameter coils. Use of the non-uniformity correction algorithm increased the similarity of all surface coil images so that the results from the 5-cm surface coil corresponded to the distribution seen with the head coil and with the 8-cm surface coil. The results from the 2.5-cm coil also showed dramatic improvements in similarity

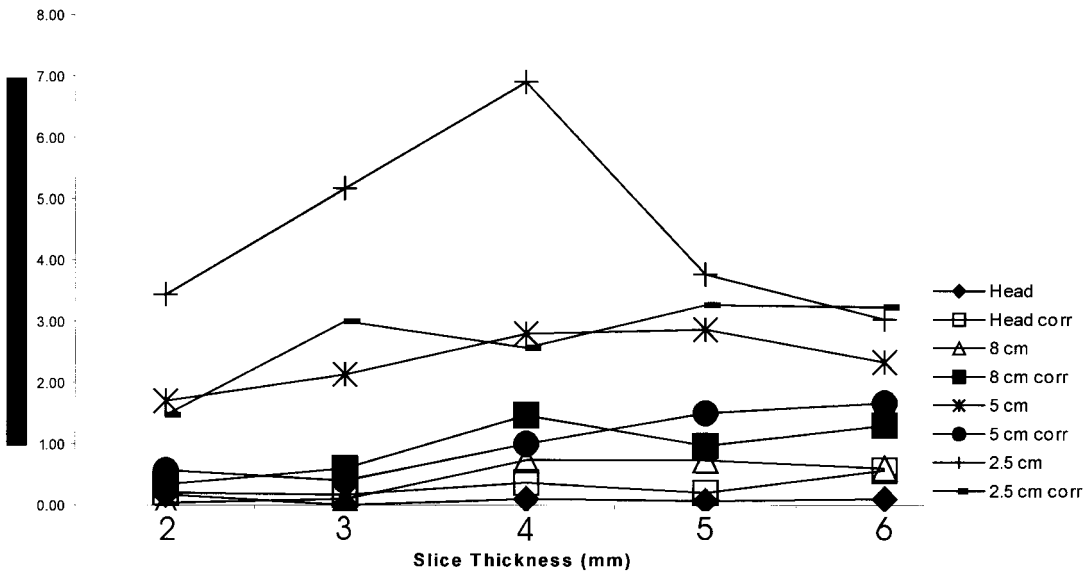

Figure 3. Plot of similarity against slice thickness. The similarity measure is calculated from the mean and variance of the signal intensities in two regions of interest in the superficial and deep parts of the vitreous humor. These were used to calculate the position at which the distributions of the regions of interest overlap. This measurement is expressed in units of SD from mean intensity of the second region of interest (deep in the globe). The distance between distributions tends to zero with increased similarity.

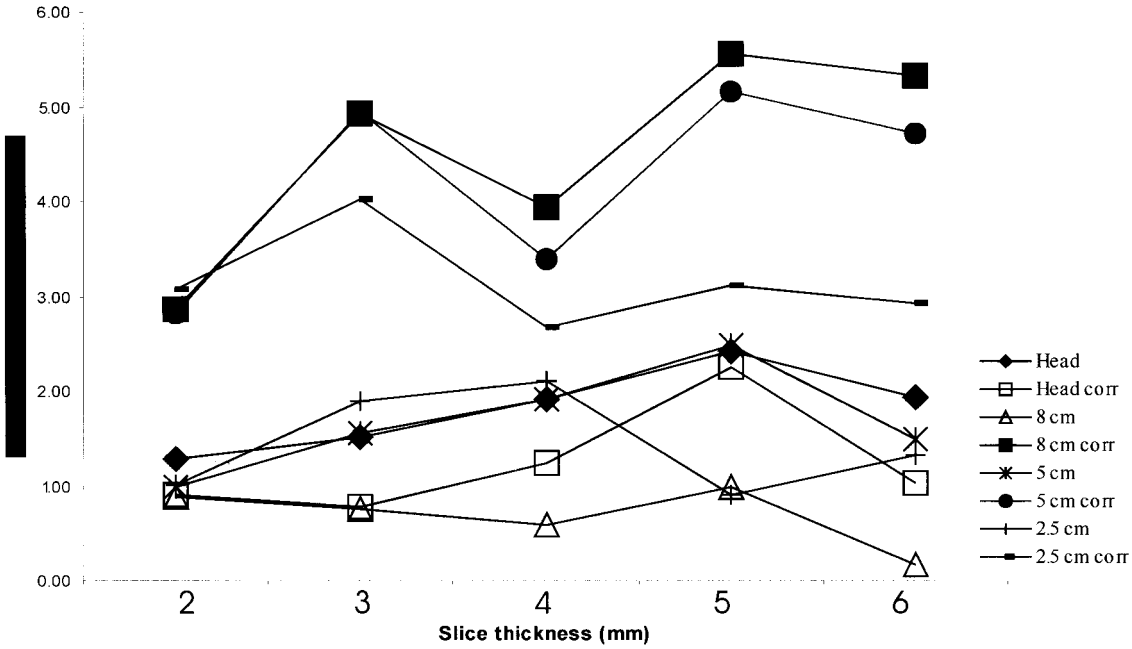

Figure 4. Plot of conspicuity against slice thickness. The conspicuity measure is calculated from the mean and variance of the orbital fat and temporalis muscle at points equidistant from the orbital surface. These were used to calculate the position at which the signal intensity distributions of the regions of interest overlap. This measurement is expressed in units of SD from mean intensity of the temporalis. The distance between distributions becomes greater with higher conspicuity.

so that the distribution was similar to the images obtained with the uncorrected 5-cm diameter coil (Fig. 4). Similar effects were seen with the measurements of conspicuity obtained from the temporalis muscle and orbital fat. These tissues were chosen because they lie approximately equidistant from the plane of the surface coil and should be clearly distinguishable on the basis of signal intensity on T1, weighted images. The measurements of conspicuity produced are fascinating and provide considerable insight into the way in which intensity drop off can affect the ability to interpret images. The conspicuity of the two tissues was effectively insignificant with all head coil and all uncorrected surface coil images. Although the eye can distinguish the tissues, the difference in intensity distribution between them was less than 3 SD from the mean intensity in all cases. Once the non-uniformity algorithm was applied, all surface coil images demonstrated conspicuities between 3 and 6 SD from the mean (Fig. 4). In the case of the head coil, the non-uniformity algorithm produced only a minor improvement in conspicuity, reflecting the high overall image uniformity produced by the coil. The improvement of conspicuities seen in corrected surface coil images results from narrowing the signal intensity distribution due to reduction of signal drop-off as the distance from the coil increases. The effect of the correction algorithm on surface coil images is therefore a reduction in the component of the image noise that results from signal drop-off while maintaining the benefits of the true increases in signal-to-noise ratio provided by the surface coil. Effectively the algorithm applies the optimal non-linear windowing parameters to the image on a pixel-by-pixel basis to minimize the dynamic range of the intensity distribution for any homogeneous tissue.

Assessing the effect of the intensity non-uniformity correction algorithm on the subjective appearance of the images was performed using a forced choice algorithm. The effective comparison of a large group of images with potentially minor differences presents a significant problem with opportunities for bias. The random presentation of anonymous images and the secondary construction of a rank table eliminates this bias and allows direct comparison of inter- and intra observer variation, using simple measures to estimate the reliability of the ranking system. The forced-choice technique relies on a clear definition of the characteristic to be classified. In this study, the quality of demonstration of the structures at the optic nerve head and in the cavernous sinus were chosen to represent the anterior and far posterior extents of the orbit. The measures of intra- and inter-observer variation for all comparisons showed excellent agreement indicating that the forced choice technique produced reproducible and reliable rankings of image quality. It was not surprising that the optimal image quality at the optic nerve head was provided by the smallest coil, and that the optimal image quality in the cavernous sinus was produced by the head coil. The improved ranking of all surface coil images after non-uniformity correction indicates that the algorithm does produce a genuine improvement in the clinical quality of the images, which translates to greater observer confidence. The use of the non-uniformity correction algorithm produced images from the 5-cm surface coil that had the highest overall mutual ranking from both observers. It should be appreciated that the weighted rankings represent the combined image quality at the optic nerve head and the cavernous sinus and that individual images in these area were

best obtained with the 2.5-cm and head coils, respectively.

In conclusion, the use of an intensity non-uniformity correction algorithm produced improvements in the intensity distribution of surface coil images that decreased coil induced signal drop-off with a measurable improvement in tissue conspicuities. The subjective quality of all surface coil images was significantly improved, and the optimal image quality for the whole orbit in this study was obtained with an intensity non-uniformity corrected image from a 5-cm flexible surface coil. The intensity non-uniformity correction algorithm is fully automatic and requires no prior information regarding coil construction, coil position, or sequence type. The effects of the algorithm will vary with the properties of the individual image but the algorithm allows the generation of surface coil images that optimize the benefits of the increased signal to noise ratio associated with surface coils, and is likely to be beneficial in all surface coil images.

REFERENCES

1. Lemke AJ, Hosten N, Bornfeld N, Bechrakis NE, Schuler A, Richter M, et al. Uveal melanoma: correlation of histopathologic and radiologic findings by using thin-section MR imaging with a surface coil. Radiology 1999;210:775–783.
2. Bilaniuk LT, Schenck JF, Zimmerman RA, Hart HR, Jr, Foster TH, Edelstein WA, et al. Ocular and orbital lesions: surface coil MR imaging. Radiology 1985;156:669–674.
3. Wilms G, Marchal G, Decrop E, van Hecke P, Baert A, Dralands G. Surface coil magnetic resonance imaging of the orbit at 1.5T. ROFO Fortschr Geb Rontgenstr Nuklearmed 1988;149:496–501.
4. Hosten N, Lemke AJ, Sander B, Wassmuth R, Terstegge K, Bornfeld N, et al. MR anatomy and small lesions of the eye: improved delineation with a special surface coil. Eur Radiol 1997;7:459–463.
5. Hosten N, Lemke AJ. A special surface coil for high-resolution ocular MRI. Front Radiat Ther Oncol 1997;30:20–25.
6. Duvoisin B, Zanella F, Sievers K. Imaging of the normal and pathological orbit. Eur Radiol 1998;8:175–188.
7. Atlas S, Bilaniuk L, Zimmerman R, Hackney D, Goldberg H, Grossman R. Orbit: initial experience with surface coil spin-echo MR imaging at 1.5T. Radiology 1987;164:501–509.
8. Jackson A, Fawcitt R. Orbital imaging. In: Gillespie J and Gholkar A, Editors. Magnetic resonance imaging and computed tomography of the head and neck. London: Chapman and Hall Medical; 1994. p 71–82.
9. Breslau J, Dalley RW, Tsuruda JS, Hayes CE, Maravilla KR. Phased-array surface coil MR of the orbits and optic nerves. AJNR Am J Neuroradiol 1995;16:1247–1251.
10. Wicks D, Barker G, Tofts P. Correction of intensity nonuniformity in MR images of any orientation. Magn Reson Imaging 1993;11:183–196.
11. Moyher SE, Vigneron DB, Nelson SJ. Surface coil MR imaging of the human brain with an analytic reception profile correction. J Magn Reson Imaging 1995;5:139–144.
12. Ozkan M, Dawant B, Maciunas R. Neural-network based segmentation of multi-modal medical images: acomparative and prospective study. IEEE Trans Med Imaging 1993;12:534–544.
13. Dawant B, Zijdenbos A, Margolin R. Corrections of intensity in MR images for computer aided tissue classification. IEEE Trans Med Imaging 1993;12:770–781.
14. Wells W, Grimson W, Kikiris R, Jolesz F. Adaptive segmentation of MR data. IEEE Trans Med Imaging 1996;15:429–442
15. Vokurka E, Thacker N, Jackson A. A fast model independent method for automatic correction of intensity nonuniformity in MRI data. J Magn Reson Imaging 1999;10:582–588.
16. Wehrli F Kanal E. Orbital imaging: factors determining magnetic resonance imaging appearance. Radiol Clin North Am 1987;25:419–427.
17. Lacey A. Tina (software). Manchester: University of Manchester, Neuroimage Analysis Centre, 1999. www.niac.man.ac.uk/Tina
18. Altman D. Practical statistics for medical research. London: Chapman Hall; 1991:64–122.
19. Kulkarni M, Patton J, Price R, Technical considerations for the use of surface coils in MRI. AJR Am J Roentgenol 1986;147:373–378.
20. Atlas SW, Grossman RI, Savino PJ, Sergott RC, Schatz NJ, Bosley TM, et al. Surface-coil MR of orbital pseudotumor. AJR Am J Roentgenol 1987;148:803–808.
21. Hendrix LE, Massaro BM, Daniels DL, Smith DF, Haughton VM. Surface coil MR evaluation of a lacrimal gland carcinoma. J Comput Assist Tomogr 1988;12:866–868.